

Low-power-consumption Circuit for MEMS Thermal Wind Sensors Operated in Constant-temperature-difference Mode

Xingheng Luo, Ming Qin,* and Qing-An Huang

Key Laboratory of MEMS of the Ministry of Education, Southeast University, Nanjing 210096, China

(Received August 4, 2022; accepted April 4, 2023)

Keywords: MEMS thermal wind sensor, constant-temperature-difference (CTD) mode, low power consumption, DC/DC converter, switching mode power supply (SMPS)

In this paper, the traditional control circuit of the constant-temperature-difference (CTD) mode for a MEMS thermal wind sensor is introduced and analyzed. Then, it is demonstrated that the transistor in this closed-loop control circuit has high power consumption owing to its use as a modulator with low conversion efficiency to supply a high current for the Wheatstone bridge. To reduce unnecessary power consumption, the use of a DC/DC converter with high conversion efficiency in the switching mode power supply is proposed to replace the transistor in a new low-power-consumption control circuit of the CTD mode. Then the loop stability and the performance of the new control circuit in reducing the power consumption are verified by simulation. Finally, power-consumption experiments are performed on the traditional and new control circuits in a laminar flow wind tunnel. The experimental results show the capability of the new low-power-consumption control circuit to reduce the total power consumption of the control circuit by 20 to 40% at wind speeds from 0 to 30 m/s by replacing the transistor with the DC/DC converter.

1. Introduction

MEMS thermal wind sensors have been widely studied because of their small size, low cost, and easy fabrication.^(1–3) They typically consist of a center heater and four sensing elements arranged downstream and upstream symmetrically in two perpendicular directions.⁽³⁾ Wind information can be measured by detecting the amount of heat that has been removed from the heater or by detecting the temperature difference between the upstream and downstream sensing elements. A thermal anemometer and a calorimetric flow sensor are respectively produced on the basis of these two principles.⁽⁴⁾ Thermal wind sensors, an extension of thermal flow sensors, are commonly operated in one of two modes: constant-power (CP) mode and constant-temperature-difference (CTD) mode.^(5,6)

Because thermal wind sensors are usually applied in mobile meteorological measurement equipment and other low-power devices, it is necessary to reduce the total power consumption of thermal wind sensors. Many designs from the literature have been based on low-power-consumption research and can be categorized into two main types. The first type of design

*Corresponding author: e-mail: mqin@seu.edu.cn
<https://doi.org/10.18494/SAM4007>

reduces the heat dissipation on the chip caused by the substrate.^(7–14) Therefore, a substrate with low thermal conductivity can be used,^(7–12) and the fabrication of insulation trenches in the chip is an approach sometimes employed for this type of design.^(8,13,14) The other type of design reduces the power consumption of the processing circuit. In the design of Makinwa and Huijsing, thermal sigma-delta ($T\Sigma\Delta$) modulators and system-level chopping are adopted in the interface circuit to control the power distribution in different heating parts by employing heating pulses of different lengths with a constant total heating power.^(15,16) The power consumption of the sensor can be reduced to 25 mW with the capability of detecting airflow speeds of up to 25 m/s.⁽¹⁶⁾ The operation mode of this method is called the temperature-balanced (TB) mode, which combines the advantages of the CTD mode and the CP mode: a wide measurement range and low power consumption. However, the sensor chip is not bonded in the center of the plate; thus, the output signals are distorted.⁽¹⁷⁾ Thus, other approaches to reduce the power consumption of the processing circuit that comprises the control circuit should be employed.

A MEMS thermal wind sensor that measures the wind speed by detecting the total heat loss of the sensor chip has been developed. The heater is bonded in the center of the chip as shown in Fig. 1(a), and the fabrication of the sensor chip is shown in Fig. 1(b). The heater of this sensor is operated in the CTD mode in the control circuit to achieve a wider measurement range than that of sensors operated in the CP mode, and the power consumption of this control circuit can be reduced by circuit design. In the traditional control circuit of the CTD mode, a transistor is used in the closed-loop circuit as a modulator for the Wheatstone bridge, and the power dissipation of the transistor results in high power consumption of the whole control circuit in the processing circuit.⁽¹⁸⁾ Thus, the transistor with low conversion efficiency should be replaced by a modulator with high conversion efficiency in a new control circuit of the CTD mode to reduce total power consumption.

A DC/DC converter is usually used in the switching mode power supply (SMPS) to change the voltage level and modulate the output voltage for applications requiring high current. A DC/DC converter working stably and normally can commonly achieve over 80% conversion efficiency. Therefore, traditional modulators, such as resistance dividers and transistors, which cause large power losses, can be replaced by a DC/DC converter in the SMPS at a high current to reduce the power consumption of the circuit.^(19,20)

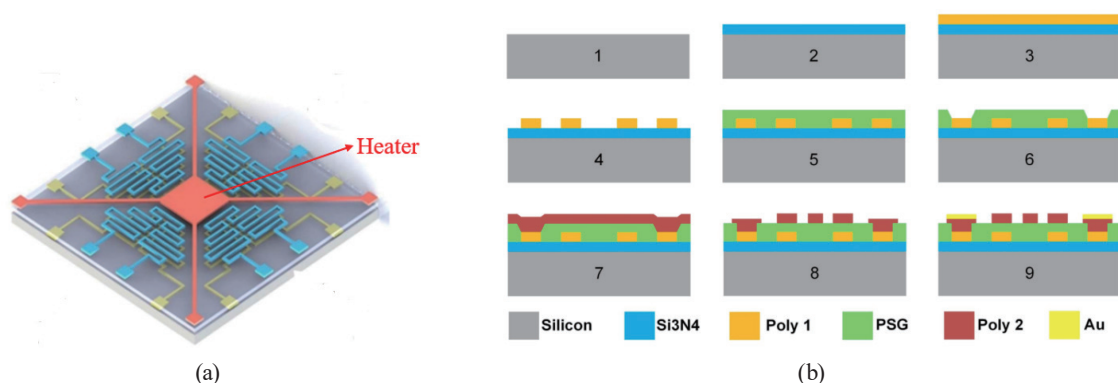


Fig. 1. (Color online) (a) Schematic of MEMS thermal wind sensor chip. (b) Fabrication process of chip.

In this paper, we present a novel low-power-consumption control circuit of the CTD mode for MEMS thermal wind sensors. In this new control circuit, we replace the traditional transistor with a DC/DC converter with high conversion efficiency to reduce the total power consumption of the control circuit. The DC/DC converter and external circuit compose the feedback loop of the SMPS, in which the output voltage is determined by the external circuit including a Wheatstone bridge with an operational amplifier for CTD control. In this way, the new control circuit can realize the functionality of a MEMS thermal wind sensor with low power consumption.

Although low power consumption design by the SMPS is a circuit technology that is already developed and employed to supply power to the bridge,⁽²¹⁾ it is the first time to employ it in the control circuit for the thermal wind sensor, which needs the dynamic output of a DC/DC converter to control the dynamic supply voltage of the bridge under different balanced conditions for a constant overtemperature. This is meaningful and useful to other low-power-consumption research studies on the closed-loop circuit with the bridge for dynamic control under balanced conditions.

2. Principle and Method

2.1 Traditional CTD control circuit for thermal wind sensor

The heater is controlled at a constant temperature above the temperature of wind by a traditional control circuit of the CTD mode, which is shown in Fig. 2. R_c is a temperature sensor of the same material as heater R_h , and the ratio between the resistances of resistors R_1 and R_c determines the overtemperature of the heater. The functionality of the circuit is described as follows. First, after the Wheatstone bridge is supplied by a voltage drop over resistor R_3 , there is

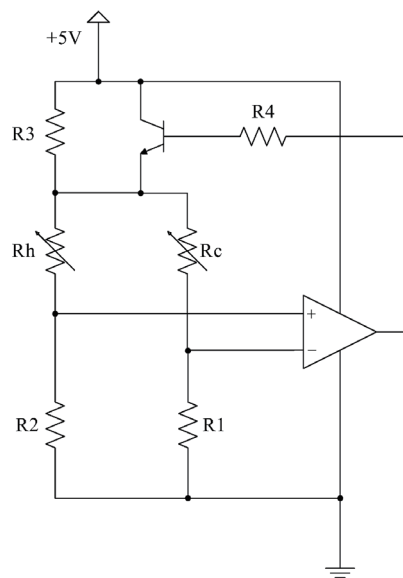


Fig. 2. Traditional control circuit with a transistor for the CTD mode operation of a MEMS thermal wind sensor.

a measurable bridge voltage, which is amplified by the operational amplifier due to the low resistance of heater R_h at air temperature. Then the supply voltage of the Wheatstone bridge is adjusted by an n–p–n transistor whose base voltage is determined by the output voltage of the operational amplifier. As a result of a rise in the supply voltage of the bridge, the temperature of the heater begins to increase, and its resistance increases until the bridge becomes balanced with the constant initial bridge supply voltage and the initial overtemperature when there is no wind. When the wind flows at a constant speed, a lower-temperature heater with a lower resistance of the bridge leads to a higher output voltage of the operational amplifier, which causes a new balanced condition where the temperature of the heater remains constant at the initial preset overtemperature. In this way, the overtemperature is controlled in the CTD mode and the wind speed can be measured from the corresponding supply voltage of the Wheatstone bridge or the output voltage of the operational amplifier.

The supply voltage of this control circuit of the CTD mode is set as 5 V, which makes it possible to change the measurement range of the wind speed as needed by presetting different initial supply voltages of the bridge when there is no wind. A high initial supply voltage of the bridge brings about a wide measurement range and high sensitivity but high power consumption. The transistor is used in the circuit as a modulator for the bridge because it can follow the change in the output voltage from the operational amplifier and deliver a high current to the Wheatstone bridge.

In actual experiments, sensor chips are fabricated by batch production, and therefore the heaters of different chips are the same. In contrast, R_1 is commonly changed to preset the initial supply voltage of the bridge and the overtemperature of the heater while fixing the resistance of R_2 . Because the wind speed is measured by detecting the total heat loss of the sensor in the CTD mode, the power consumption of the heater P follows King's law:⁽²²⁾

$$P = (A + BV^n) \cdot \Delta T, \quad (1)$$

where A and B are constant values determined by the thermodynamic parameters of air and the dimension parameters of objects, n is 0.5 when the wind is a laminar flow, V is the wind speed, and ΔT is the overtemperature of the heater, which is determined by the bridge supply voltage. As a result, P has exactly the same value for the same bridge supply voltage in different sensors as other values in Eq. (1) are correspondingly the same in different sensors from the same batch. Therefore, after the initial bridge supply voltages of different sensors are set to be the same under a balanced condition by adjusting the Wheatstone bridge when there is no wind, the overtemperature ΔT , the measurement range, and the measurement sensitivity also become the same. Consequently, when the wind speed is measured, the same supply voltage of the bridge in different sensors whose heaters are preset to the same overtemperature means that the same wind speed is obtained.

As a resistor used for dropping voltage to supply the bridge with reduced power to turn on the control circuit, resistor R_3 has a much larger resistance than other resistors, which means that the current passing the transistor is approximately equal to the total bridge current I_G . According

to the traditional control circuit in Fig. 2, the power dissipation of the transistor P_T is determined by the bridge supply voltage U_S and the total bridge current I_S as follows:

$$P_T = (5 - U_S) \cdot I_S. \quad (2)$$

For different supply voltages of the bridge, the total power consumption of the traditional control circuit and the power dissipation of the transistor with the occupation percentage can be measured as shown in Fig. 3. It is clear that a transistor acting as a modulator to supply a high current for the Wheatstone bridge causes a large loss of power relative to the total power consumption, especially for a low supply voltage of the bridge, which means a low wind speed as introduced earlier. Thus, the transistor should be replaced by another type of modulator with high conversion efficiency for a high current in a new control circuit.

2.2 Low-power-consumption CTD control circuit for thermal wind sensor

We present the possibility of a low-power-consumption CTD control circuit for a MEMS thermal wind sensor to reduce power dissipation in the transistor and the total power consumption of the control circuit. In this new control circuit, the traditional transistor is replaced with an SMPS with an MP2359 switch-mode DC/DC converter, which has high conversion efficiency.

The output voltage of the DC/DC converter is determined by the relationship between its output voltage and the feedback voltage in a stable loop system. This relationship can be adjusted via the output of the operational amplifier from the traditional control circuit. In this way, the traditional transistor can be replaced by a DC/DC converter with high conversion efficiency for modulation with the capability of delivering a high current, which can reduce the power consumption of the whole control circuit.

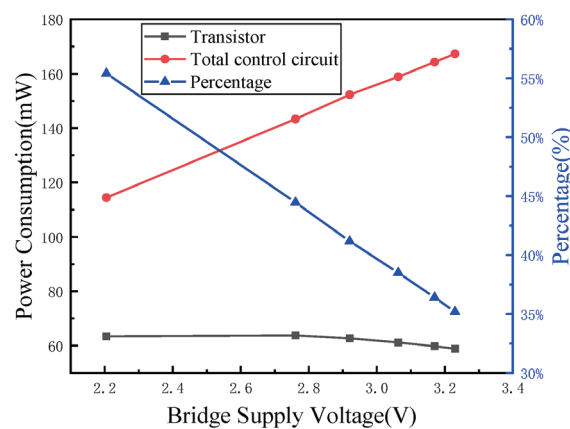


Fig. 3. (Color online) Power consumption versus bridge supply voltage in traditional control circuit.

The novel low-power-consumption control circuit of the CTD mode with a DC/DC converter is shown in Fig. 4. The input voltage of the converter is the same as the supply voltage of the whole control circuit, and the output voltage of the converter is used as the supply voltage of the Wheatstone bridge. The output of the operational amplifier, which represents the wind speed, is connected to a diode to prevent a reverse current. A compensation capacitor is connected between the input and output of the operational amplifier for phase compensation of the whole feedback loop to eliminate oscillation. Then the external resistance divider circuit of the converter, which is most frequently used in the feedback loop of a DC/DC converter, is joined by a feedback resistor connected to the diode. As a result, the original fixed relationship between the output voltage and the feedback voltage is changed to a new relationship.

As shown in the new control circuit in Fig. 4, the node between three resistors is connected to the FB pin, and therefore, this node can be analyzed using Kirchhoff's law as follows:

$$I_2 = I_1 + I_3, \tag{3}$$

$$I_1 = \frac{U_h - U_{REF}}{R_4}, \tag{4}$$

$$I_2 = \frac{U_{REF}}{R_5}, \tag{5}$$

$$I_3 = \frac{U_{CTD} - U_{REF}}{R_{FB}}, \tag{6}$$

Thus, the bridge supply voltage U_h is given by

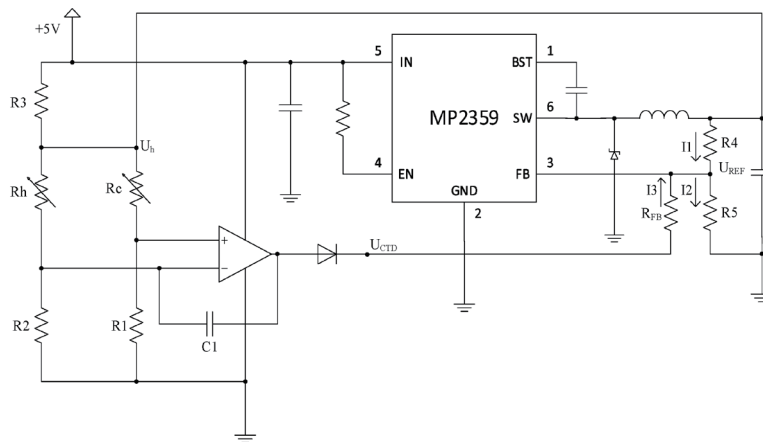


Fig. 4. New low-power-consumption CTD control circuit with a DC/DC converter.

$$U_h = U_{REF} \cdot \left(1 + \frac{R_4}{R_5}\right) + (U_{REF} - U_{CTD}) \cdot \frac{R_4}{R_{FB}}, \quad (7)$$

where U_{REF} is fixed at 0.81 V and U_{CTD} is the output voltage of the amplifier with the diode. Therefore, a new feedback close loop is constructed, and the wind speed can be measured from the bridge supply voltage.

Because the power consumption of other components is very low in comparison with the DC/DC converter and the bridge, the calculation formula for the power consumption of DC/DC converter $P_{DC/DC}$ can be given by

$$P_{DC/DC} = 5 \cdot I_{total} - U_h \cdot I_h, \quad (8)$$

where I_{total} is the total current of the control circuit and I_h is the supply current of the bridge.

It is noteworthy that there is a negative correlation between the supply voltage of the Wheatstone bridge and the output voltage of the operational amplifier in this circuit rather than the positive correlation in the traditional control circuit. Therefore, another important difference in this new circuit is the exchange of the connection between the bridge and the inputs of the operational amplifier. In addition, the approach to set the initial supply voltage of the bridge and the overtemperature of the heater in the new circuit follows the same principle in the traditional circuit by adjusting the Wheatstone bridge.

3. Results and Discussion

3.1 Simulations

To examine the circuit operation, the loop stability, and the performance in reducing the power consumption of low-power-consumption control circuit, we performed simulations of the new control circuit using the simulation of piecewise linear systems (SIMPLIS) software.

A model of the heater was developed in SIMPLIS, and a simplified model of the DC/DC converter was supported by its R&D company. All other parameters of the electronic components in the Wheatstone bridge and operational amplifier were set to be the same as in the traditional control circuit.

To evaluate the stability of the whole feedback loop, the loop should be evaluated by small-signal analysis with a frequency response analyzer in the simulation. In the evaluation of loop response for the SMPS, a small signal resistor was set at the output of the DC/DC converter and a small AC signal was injected into this resistor. Then, the frequency response analyzer was set in the circuit to acquire the response to the input signal, in order to obtain the relationship between the gain and phase of the SMPS loop versus the frequency. There are two feedback loops in the control circuit: the loop of the converter with the external resistance divider and the

loop of CTD control with the Wheatstone bridge and operational amplifier. These two loops compose one whole loop for the new SMPS with the capability of measuring the wind speed; thus, the stability of the whole loop can be analyzed using the stability criterion of the SMPS.⁽²³⁾

In the actual simulation performed to evaluate the loop stability, an external small perturbation signal was injected into the SMPS loop connected to an inserted resistor, and the Bode plot shown in Fig. 5 was obtained by the frequency response analyzer.

As shown in Fig. 5, the phase margin is around 53.3° , which is over 45° , the gain margin is around 22.2 dB, which is over 12 dB, and the crossover frequency is 124.3 kHz, which is between $1/20$ and $1/6$ of the switching frequency of 1.4 MHz.⁽²³⁾ Therefore, the whole SMPS loop is sufficiently stable according to the stability criterion of the SMPS.

To evaluate the performance of the low-power-consumption control circuit in reducing power consumption, we performed a simulation to monitor the power consumption of the control circuit and DC/DC converter, the results of which are shown in Fig. 6. The bridge supply voltage of the control circuit was set as correspondingly the same value as in Fig. 3.

3.2 Experiments

Figure 7(a) shows a microphotograph of the MEMS wind sensor chip, and it was packaged as shown in Fig. 7(b). The packaged wind sensor chip and the whole processing circuit implemented on a printed circuit board were installed in a protective shell as shown in Fig. 7(c). Then the shell was installed in a laminar flow wind tunnel to perform measurement as shown in Fig. 7(d). The wind tunnel can provide wind speeds of up to 33 m/s. During the experiments, two types of processing circuit, the traditional control circuit and the low-power-consumption control circuit, operated sensors for measurements. Then the same initial bridge supply voltage was set for these

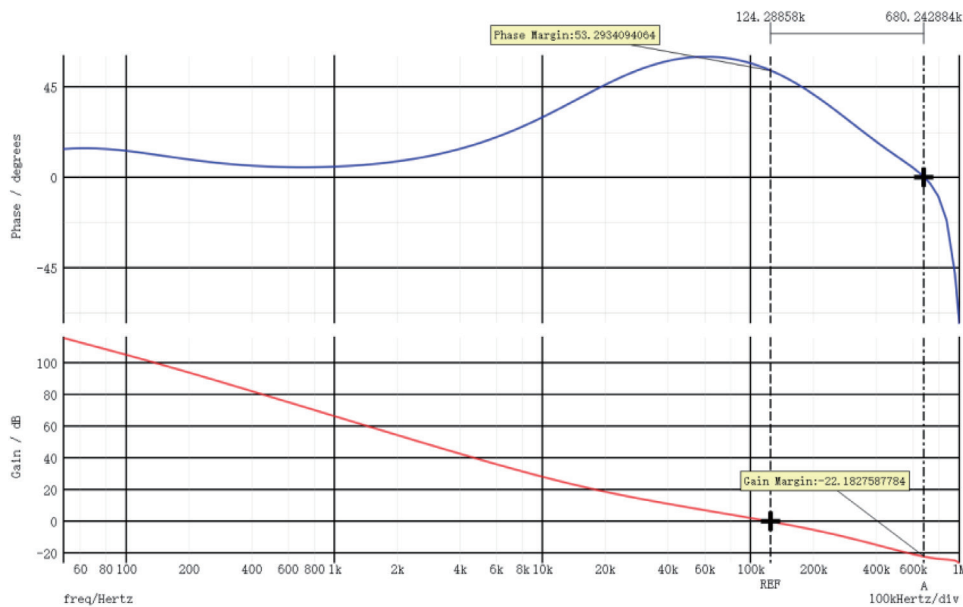


Fig. 5. (Color online) Bode plot obtained from small-signal analysis with frequency response analyzer.

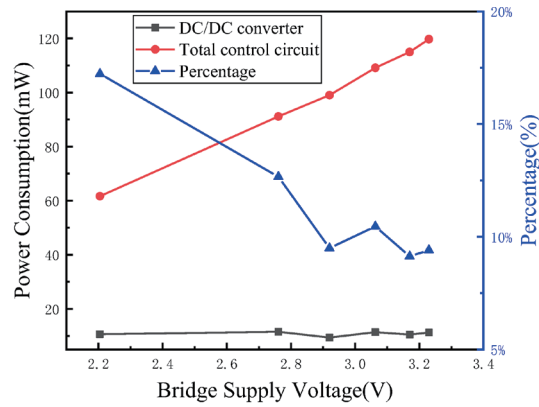


Fig. 6. (Color online) Simulated power consumption versus bridge supply voltage in low-power-consumption control circuit.

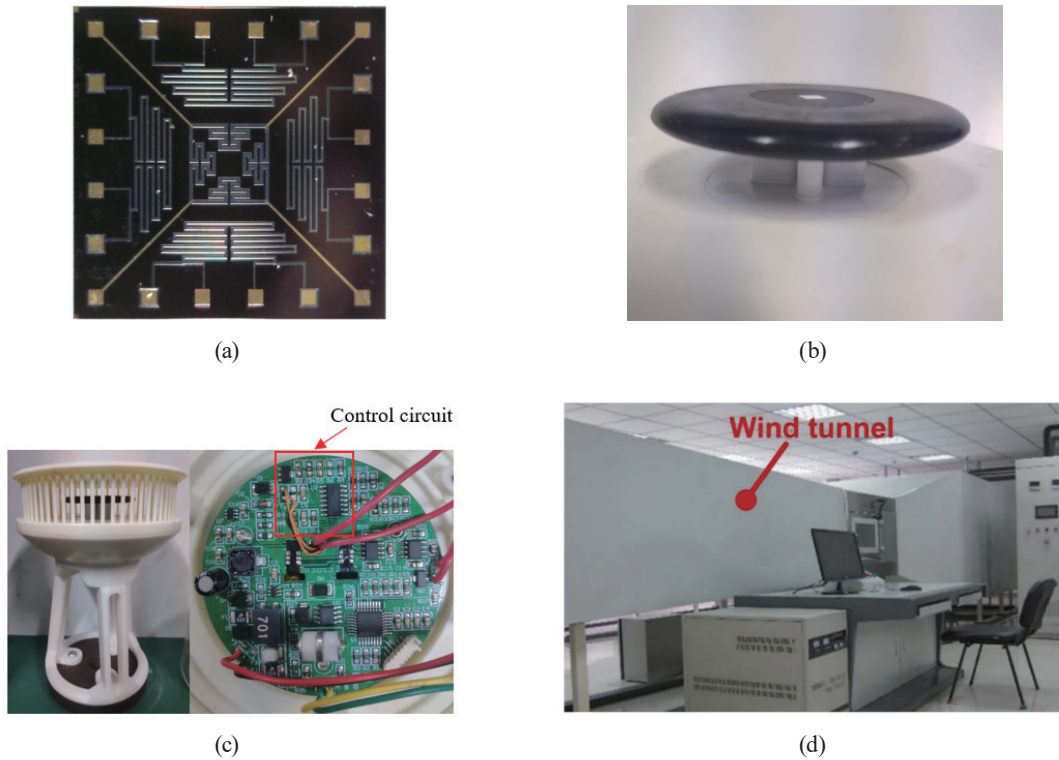


Fig. 7. (Color online) (a) Microphotograph of MEMS thermal wind sensor chip. (b) Packaged wind sensor chip. (c) MEMS thermal wind sensor with control circuit. (d) Wind tunnel in experiment.

two types of control circuit by adjusting the Wheatstone bridge as introduced in the traditional control circuit when there was no wind, then measurements were performed in the wind tunnel with the same wind speed. During the experiments performed in the wind tunnel, the bridge supply voltages were processed and calculated using the processing circuit to obtain wind speed information. In addition, the power consumption of these two types of control circuit was

detected and calculated from the measuring current and voltage in different parts of the control circuit.

The total power consumption of the control circuit and the power dissipation of the transistor with the occupation percentage are shown for the wind sensor operated by the traditional control circuit in Fig. 8(a). The transistor in the traditional control circuit has much power loss relative to the total power consumption, especially at a low wind speed.

The total power consumption of the control circuit and the power consumption of the DC/DC converter with the occupation percentage for the wind sensor operated by the new control circuit are shown in Fig. 8(b). The distinct contrast between the two results and the percentage reduction of the total power consumption for the new control circuit are shown in Fig. 8(c). The result shows the capability of the new control circuit to reduce the total power consumption of the control circuit by 20 to 40% at wind speeds from 0 to 30 m/s. The percentage reduction of the power consumption is high at low wind speeds and gradually decreases with increasing wind speed.

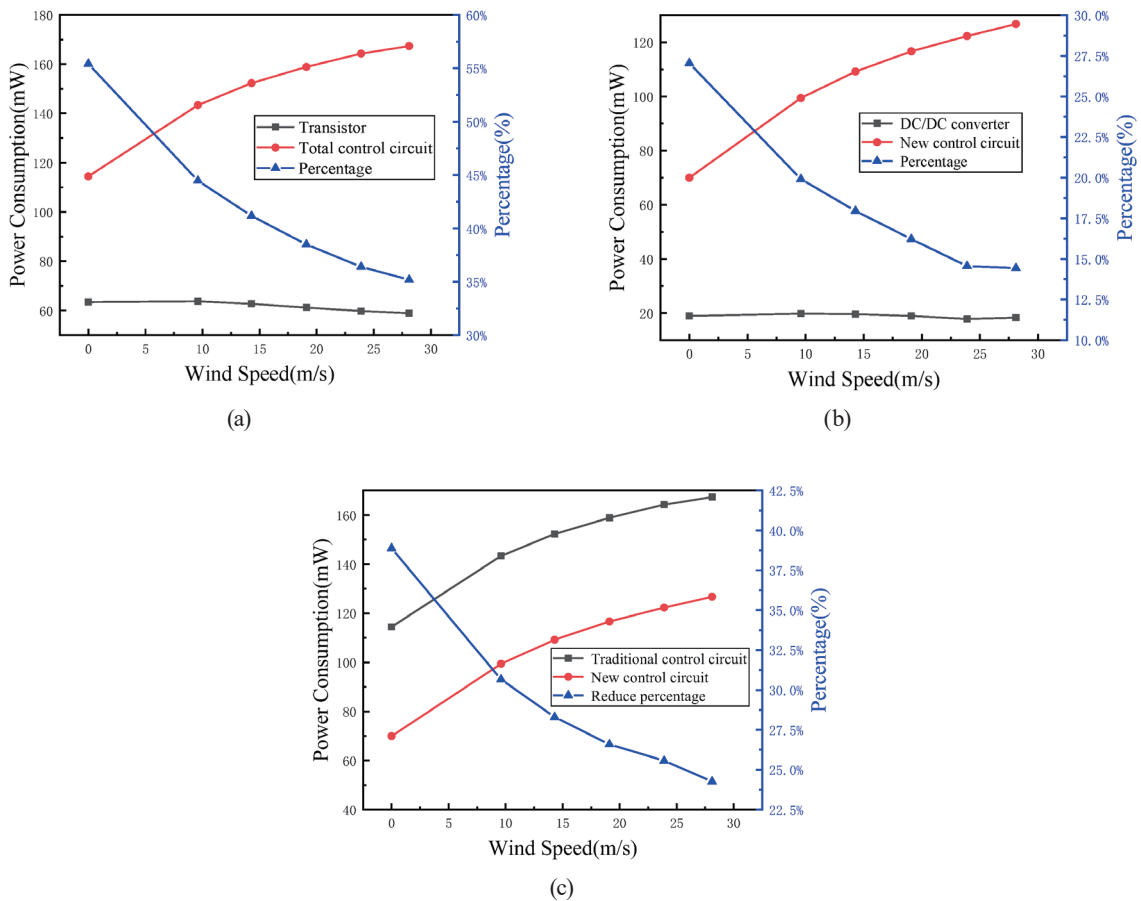


Fig. 8. (Color online) Experimental results for power consumption of control circuit for thermal wind sensor in wind tunnel. (a) Power consumption versus wind speed in traditional control circuit. (b) Power consumption versus wind speed in low-power-consumption control circuit. (c) Comparison of power consumption of low-power-consumption control circuit and traditional control circuit.

4. Conclusions

In this paper, we presented a novel low-power-consumption control circuit of the CTD mode for MEMS thermal wind sensors in which the transistor with low conversion efficiency is replaced by a DC/DC converter with high conversion efficiency. Simulation results showed the stability of the new feedback closed-loop circuit and the performance of the new control circuit in reducing power consumption. Experimental results showed the capability of the new control circuit in markedly reducing the power consumption by replacing the traditional transistor. This proposed research could be helpful for studies on low-power-consumption MEMS thermal wind sensors.

Acknowledgments

This work was supported by the Key R&D Program of Shandong Province and Major Technological Innovation Project (Project No. 2020CXGC010203). The authors would like to thank Bo Qi and Tian Zhao for their support.

References

- 1 N. T. Nguyen: Flow Meas. Instrum. **8** (1997) 7. [https://doi.org/10.1016/S0955-5986\(97\)00019-8](https://doi.org/10.1016/S0955-5986(97)00019-8)
- 2 H. Baltes and O. Paul: Proc. IEEE **86** (1998) 1660. <https://doi.org/10.1109/5.704271>
- 3 J. Kuo, L. Yu, and E. Meng: Micromachines **3** (2012) 550. <https://doi.org/10.3390/mi3030550>
- 4 J. Z. Zhang, Z. F. Zhou, M. Qin, and Q. A. Huang: J. Micromech. Microeng. **30** (2020) 125001. <https://doi.org/10.1088/1361-6439/abb993>
- 5 G. P. Shen, M. Qin, and Q. A. Huang: Microsyst. Technol. **15** (2009) 279. <https://doi.org/10.1007/s00542-008-0665-5>
- 6 T. Lammerink, N. R. Tas, G. Krijnen, and M. Elwenspoek: Proc. IEEE 13th Annu. Int. Conf. Micro Electro Mechanical Systems (2000). <https://doi.org/10.1109/memsys.2000.838572>
- 7 G. Kaltsas and A. G. Nassiopoulou: Sens. Actuators, A **76** (1999) 133. [https://doi.org/10.1016/S0924-4247\(98\)00370-7](https://doi.org/10.1016/S0924-4247(98)00370-7)
- 8 Y. Q. Zhu, B. Chen, M. Qin, J. Q. Huang, and Q. A. Huang: J. Micromech. Microeng. **25** (2015) 085011. <https://doi.org/10.1088/0960-1317/25/8/085011>
- 9 G. P. Shen, M. Qin, and Q. A. Huang: IEEE Sens. J. **10** (2009) 340. <https://doi.org/10.1109/JSEN.2009.2034625>
- 10 R. Vilares, C. Hunter, I. Ugarte, I. Aranburu, J. Berganzo, J. Elizalde, and L. J. Fernandez: Sens. Actuators, B **147** (2010) 411. <https://doi.org/10.1016/j.snb.2010.03.054>
- 11 R. Zhu, P. Liu, X. D. Liu, F. X. Zhang, and Z. Y. Zhou: IEEE Int. Conf. Micro Electro Mechanical Systems (2009). <https://doi.org/10.1109/memsys.2009.4805435>
- 12 T. Glatzl, H. Steiner, F. Kohl, T. Sauter, and K. Franz: Sens. Actuators, A **237** (2016) 1. <https://doi.org/10.1016/j.sna.2015.11.016>
- 13 D. H. Gao, M. Qin, H. Y. Chen, and Q. A. Huang: Proc. 7th Int. Conf. Solid-State and Integrated Circuits Technology (2004). <https://doi.org/10.1109/icsens.2004.1426311>
- 14 Y. Ye, Z. Yi, S. Gao, Q. Ming, and Q. A. Huang: IEEE Sens. J. **17** (2017) 8324. <https://doi.org/10.1109/JSEN.2017.2766121>
- 15 K. Makinwa and J. H. Huijsing: IEEE Sensors (2005). <https://doi.org/10.1109/icsens.2005.1597757>
- 16 J. Wu, C. V. Vroonhoven, Y. Chae, and K. Makinwa: IEEE Sensors (2011). <https://doi.org/10.1109/ICSENS.2011.6127204>
- 17 S. P. Matova, K. Makinwa, and J. H. Huijsing: IEEE Sens. J. **3** (2004) 761. <https://doi.org/10.1109/JSEN.2003.820324>
- 18 C. Sosna, R. Buchner, and W. Lang: IEEE Trans. Instrum. Meas. **59** (2010) 1715. <https://doi.org/10.1109/TIM.2009.2025988>

- 19 Z. Iqbal, U. Nasir, M. T. Rasheed, and K. Minir: IEEE Int. Conf. Environment and Electrical Engineering (2015). <https://doi.org/10.1109/EEEIC.2015.7165299>
- 20 Z. Zhu and Y. Yang: Research and Progress of Sse Solid State Electronics (2008).
- 21 K. Tatehara, Y. Shiiki, S. Nakagawa, T. Tanaka, and H. Ishikuro: 2020 IEEE Int. Symp. Circuits and Systems (ISCAS) (2020). <https://dx.doi.org/10.1109/iscas45731.2020.9180618>
- 22 L. V. King: Philos. Trans. Royal Soc. A **214** (1914). <https://doi.org/10.1098/rsta.1914.0023>
- 23 Y. Panov and M. Jovanovic: 19th Annu. IEEE Applied Power Electronics Conference and Exposition (APEC '04, 2004). <https://doi.org/10.1109/tpel.2005.850926>

About the Authors



Xingheng Luo received his B.S. degree in electronics engineering from Southeast University, Nanjing, China, in 2019, where he is currently pursuing his M.S. degree in electronics engineering. His current interests include MEMS design, low-power design, application research, and thermal wind sensors. (xingheng.luo@outlook.com)



Ming Qin (Member, IEEE) received his B.S. degree in electrical engineering from Wuxi Institute of Technology, Wuxi, China, in 1988, and his M.S. and Ph.D. degrees in electrical engineering from Southeast University, Nanjing, China, in 1994 and 1997, respectively. After graduation, he joined the Department of Electronic Engineering, Southeast University as an assistant professor, where he became an associate professor in 1999 and a full professor in 2003. He was a post-doctoral researcher with Hong Kong University of Science and Technology, Hong Kong, in 1999. He has served as the director of CMOS MEMS Branch, Key Laboratory of MEMS, Ministry of Education, Southeast University. He has authored over 30 peer-reviewed international journal/conference papers and holds more than 20 Chinese patents. (mqin@seu.edu.cn)



Qing-An Huang (Fellow, IEEE) received his B.S. degree from Hefei University of Technology, Hefei, China, in 1983, his M.S. degree from Xidian University, Xi'an, China, in 1987, and his Ph.D. degree from Southeast University, Nanjing, China, in 1991, all in electronics engineering. His Ph.D. research was focused on micromachined GaAs piezoelectric sensors. After graduation, he joined the Department of Electronic Engineering, Southeast University as a faculty member, where he became a full professor in 1996 and was appointed as a Chang-Jiang Scholar by the Ministry of Education in 2004. He served as the founding director of the Key Laboratory of MEMS, Ministry of Education, Southeast University from 2001 to 2018. He authored the book Silicon Micromachining Technology (Science Press, 1996), edited the book Micro Electro Mechanical Systems (Springer, 2018), and authored or coauthored four book chapters and over 200 peer-reviewed international

journal/conference papers, and he holds over 120 Chinese patents. Dr. Huang is an editorial board member of the *Journal of Micromechanics and Microengineering*. He was a recipient of the National Outstanding Youth Science Foundation Award of China in 2003. He was the co-chair of the SPIE Microfabrication and Micromachining Process Technology and Devices Conference (Proceedings of SPIE, vol. 4601, 2001), a TPC co-chair of the Sixth Asia-Pacific Conference of Transducers and Micro/Nano Technologies (APCOT) (Nanjing, 2012), and a TPC member of TRANSDUCERS from 2009 to 2019 and the IEEE Sensors Conference from 2002 to 2016. He served as the steering committee chair of APCOT from 2012 to 2014. He has been the editor-in-chief of the Chinese Journal of Sensors and Actuators since 2005. (hqa@seu.edu.cn)